A DFT exploration of the organization of thiols on Au(111): a route to self-assembled monolayer of magnetic molecules†

Gopalan Rajaraman,‡ Andrea Caneschi, Dante Gatteschi and Federico Totti*

Nitronyl nitroxides with thiol groups, NitRs, provide exciting opportunities for investigating the properties of magnetic SAMs on gold surfaces. Here we have employed periodic/molecular DFT calculations to study the energetics, structure, bonding and magnetic exchange of SAMs of nitronyl nitroxide radical thiols on Au(111). Two structures 4-(methylthio)phenyl nitronyl nitroxide (NitR-**A**-SCH$_3$), **A** = phenyl, and 4-(methylthio)methyl phenyl nitronyl nitroxide (NitR-**B**-SCH$_3$), **B** = phenyl-CH$_2$, have been chosen. The radical species of type NitR-**B**-S• is found to be energetically favourable with the reconstructed 1 : 2 Au$_{ad}$/thiols ratio model being the most favored structure. The computed structures are consistent with the experimental data (STM, ToF-SIMS and EPR) reported earlier. The computed magnetic exchange interactions in the SAMs of nitronyl nitroxide radicals reveal a stronger than expected intramolecular coupling, revealing the non-innocent nature of the gold surface.

1. Introduction

Self-assembled monolayers (SAMs) of functionalized organic/inorganic moieties have a great potential for applications in nanoproduction, spintronics, biological sensing, *etc.*[1–7] Single atoms or molecules once grafted onto a metal surface can keep their peculiar behaviour as in the isolated phase and/or can exhibit different and unprecedented properties from the bulk/isolated ones. Such properties can range from the coupling of the SAMs with the electronic and optical properties of a metallic surface to the linking of macroscopic interfacial phenomena to molecular-level structures.[3]

Magnetic properties have long been neglected but recently several attempts have been made to assemble layers of Single Molecule Magnets (SMMs) with alkylthiol groups in a bottom up approach to explore the possibility of using them to build magnetic memory banks.[8–15] SMMs are molecules whose magnetization relaxes so slowly to present magnetic hysteresis associated to the individual molecules. It is therefore possible to store information in one molecule. In order to have the SMM addressable, one possibility is to organize them in SAMs using thiol derivatives for grafting them on gold surfaces. In one case it was shown that SMM behaviour can be observed in SAM at low temperature.[15]

Exciting as these systems can be, they are rather complex and a deep understanding of the substrate–magnetic molecule interaction is still very difficult. In order to gain deeper insight SAMs of simpler magnetic molecules, like nitronyl nitroxide radicals (NitRs), on gold were reported.[16–20] The advantage of the NitR is

that the R groups are easily varied and the radical moiety is a sensitive probe of redox processes occurring on the metal surface. Among several derivatives studied the 4-(methylthio)phenyl nitronyl nitroxide (**A**) and 4-(methylthio)methyl phenyl nitronyl nitroxide (**B**) (see Scheme 1) form stable and ordered SAMs[16] which keep the radical nature on the gold surface. The use of a stable radical can not only provide information on the structural arrangement of the thiols on the metal surface but also on the dynamics of the organized molecules. We decided to tackle the problem with a state-of-the-art theoretical treatment in order to rationalize a large number of experimental data available on SAM of thiols.

This work focuses on the studies on the nitronyl nitroxide radical thiols grafted on Au(111). Here we have employed the theoretical tools to gain in-depth understanding on the structure and magnetic properties of these systems. The knowledge gained from the studies on the methyl and higher alkyl thiols[21] have been utilised to get to the structure of the SAMs of NitR. The obtained structure of SAMs was then employed for the calculation of magnetic properties. We would like to note here that understanding the magnetic properties of SAMs, particularly how the electronic spin of the radical moiety is delocalised on Au(111), is very important if one wants to develop spintronics devices based on the NitRs.
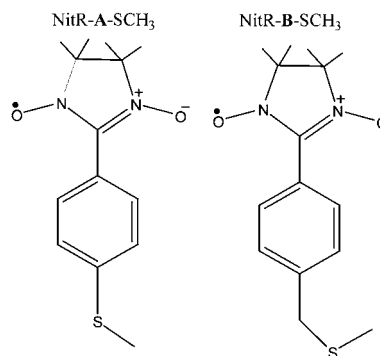
Dipartimento di Chimica, Polo Scientifico, INSTM, Università degli Studi di Firenze, via della Lastruccia 3, 50019 Sesto fiorentino, Italy. E-mail: federico.totti@unifi.it

Scheme 1

2. Computational details

All calculations have been performed with DFT implemented in CP2K program package[22–24] unless otherwise stated. The CP2K package adopts a hybrid basis set formalism known as Gaussian and Plane Wave Method[22] (GPW) where the Kohn–Sham orbitals are expanded in terms of contracted Gaussian type orbitals (GTOs), while an auxiliary plane wave basis set is used to expand the electronic charge density. A double-ζ GTH basis set and their relativistic norm-conserving pseudo potentials (Goedecker, Teter, and Hutter)[24] optimized for BLYP were used in addition to a plane wave basis set with an energy cut-off of 350 Ry. The cut-off value has been estimated by performing a series of single point calculations on a 36 atom gold cell comprising 12 gold atoms in each layer, with different cut-off values until no significant variation in the computed energy were observed. A study on the adsorption of amine compounds on a Au(111) revealed that a basis set with the similar quality to ours introduces only a minimal BSSE errors and therefore here we have not attempted to perform counterpoise corrections.[25]

TPSS[26] functional has been used throughout the calculations preformed with CP2K package.

The validity of the CP2K package as accurate Γ-point only approach has been validated through a systematic supercell approach for the calculation of transition metal surface properties.[27,28] Three different unit cells comprising 36, 56 and 90 gold atoms have been built and employed throughout the study. The unit cells were shaped to obtain in all cases three layers of Au(111) surface when the period boundary conditions are imposed over an orthorhombic simulation cell. The reconstruction of the Au(111) surface[6,21] has been simulated by positioning one or two adatoms on the top of the first layer and in all cases the adatoms positions are relaxed without any constraints to their positions. The convergence criteria of 1×10^{-7} Hartree for the SCF energy and 9×10^{-4} Hartree Å^{-1} (Hartree per Radians) for the energy gradient had been employed throughout.[28,29] The simulation cell has been defined with x and y axes on the surface plane as the reference axis. The cell size along the z axis was chosen to be 40 Å compared to an inter-layer distance of 2.35 Å. An empty space of *ca.* 20 Å is therefore left to prevent spurious inter cells polarization effects. Unless otherwise stated in all calculations the gold layer has been kept frozen. The binding energies were computed according to the following expression:[30]

$$\Delta E_{ads} = \frac{1}{nSR_1R_2}[E(nR_1R_2S - nAu_{ad}Au(111)) - E(Au(111)) + (-nSR_1R_2) \times E(SR_1R_2) - nAu_{ad} \times E(Au_{bulk})]$$

where nSR_1R_2 is the number of adsorbed alkanethiols, $E(R_1R_2S\text{-}Au(111))$ is the energy of chemisorbed species on the Au(111), $E(Au(111))$ is the energy of clean Au(111) surface, $E(SR_1R_2)$ is the energy of unadsorbed alkanethiols and $E(Au_{bulk})$ is the total energy of one gold atom in the bulk phase and the ΔE_{ads} being the formation energy for the adsorption process. nAu_{ad} are the number of gold adatoms considered in the cell. By this definition, negative ΔE_{ads} values indicate an exothermic process. The three-layer thickness of the model has been justified by calculating the enthalpy of formation of one adatom and a vacancy with respect to three, four and five layers on the 36 gold atom cell. The choice of the model with three layers *vs.* five layers introduces *ca.* 5 kcal

mol^{-1} error on adatom energy formation and 0.2 kcal mol^{-1} error on vacancy formation. Considering a large gain in the computational cost, the obtained differences are modest. Moreover the differences observed are expected to be nearly constant for the calculation of reaction energies for the current studied system. Therefore here we have chosen to study the system with three layer models.

The calculation of magnetic exchange on the NitR on the gold surface has been computed using Jaguar[31] suits of packages with a hybrid B3LYP[32] functional together with a LACVP* basis set on the CP2K computed geometries. The LACVP* basis set comprise LanL2DZ*[33] basis set for gold and 6-31G* basis set for other atoms.[34] Single point calculations have been performed with a very tight energy cut-off of 5×10^{-8} as required for such calculations.[35]

3. Results and discussion

We have previously reported experimental studies on the NitRs on Au(111).[16] In this report as an initial step for understanding the properties of organized magnetic molecules SAMs of several NitR compounds have been prepared, functionalised with thiol at their tails,[16–20] and thoroughly characterised using several experimental techniques[16] (ToF-SIMS (Time-of-Flight Secondary Ion Mass Spectrometry), STM and EPR).

The ToF-SIMS spectra of the SAMs of two nitronyl nitroxide species (NitR-**A**-SCH$_3$ and NitR-**B**-SCH$_3$, see Scheme 1 for the structures) reveal a lower order in the former. This is related to the stability and the formation energies of the two species adsorbed on the Au(111). The STM images confirm the ToF-SIMS data, while the EPR data of the SAM undoubtedly confirm that the species is intact and NitR radical nature is retained as the hyperfine and **g**-tensor of the species are only slightly perturbed upon adsorption.

We have now performed calculations on these two species to understand the structure and magnetic properties and to verify if the experimental ordering of the stabilisation could also be reproduced in order to validate the computational approach employed.

Unreconstructed surface

The first question to answer is the nature of the interaction, *i.e.*, whether the S–CH$_3$ bond undergoes a homolytic cleavage leaving an energetically favourable radical species or undergoes no changes and adsorbs as such (uncleaved). The idea of cleavage stems from the cleavage of S–H bonds in CH$_3$SH thiol on Au(111). Many theoretical and experimental evidence support a homolytic cleavage.[21,36] A very recent experimental evidence based on X-ray photoelectron spectroscopy on the SAMs of some nitroaromatic thiols prepared by vacuum vapour deposition technique conclusively reveals the S–H cleavage and the reaction of the hydrogen with one of the nitro groups.[36] Likewise the S–H bonds and the S–C bonds of the thiols are also expected to cleave. This is expected as the bond dissociation energy (BDE) of the S–C bonds (S–CH$_3$) is much lower than that of the S–H bonds in methyl thiols. This idea has been extensively tested with several dialkyl thiols and a favourable dissociation of S–C bond had been discovered.[21] Our preliminary kinetic studies also reveal

a comparable barrier heights[37] on both cases. Additionally, Surface Enhanced Raman Spectroscopy (SERS) studies for the dimethyl sulfide on gold reveal that the S–C bonds upon adsorption are found to be weaken upon adsorption while on silver surface even the S–C cleavage have been detected.[38]

Our initial calculations on the isolated species NitR-**A**-SCH$_3$ yield a formation energy of +5.3 kcal mol^{-1} for the undissociated species while for the dissociated radical the formation energy is −17.0 kcal mol^{-1} (singlet state, see below). The formation of a diradical species NitR-**A**-S• is also supported by experiments on the SAMs from a disulfide precursor.[39,40]

The unpaired electron on the sulfur head group resulting from the homolytic cleavage of the S–C bond can couple with the one delocalized on the N–O NitR orbitals giving rise to triplet and singlet (^{3,1}NitR-**A**-S•) states. In NitR-**A**-S•, the singlet state is found to be the ground state with the triplet lying only 0.7 kcal mol^{-1} above in energy. The optimised structure of the singlet species is shown in Fig. S1† with the selected structural parameters given in Table 1. Both the singlet and triplet structures adopt a fcc bridge configuration with a short and a long Au–S bond of 2.49 Å and 3.25 Å, respectively (see Table 1).

The NitR-**B**-SCH$_3$ has the formation energy of −4.1 kcal mol^{-1} whereas the dissociated radical species has the formation energy of −22.6 kcal mol^{-1} (for ^{1}NitR-**B**-S•, see Fig. S1† for the optimised structures). The singlet–triplet energy difference here is 1.6 kcal mol^{-1}, the singlet being the ground state. For species **A** the same gap is lower. Both ^{1,3}NitR-**B**-S• species adopt a fcc bridge configuration with two Au–S bonds of ∼2.58 and ∼2.79 Å long (see Table 1). The bond lengths are significantly different from those of the corresponding species of **A** and this is essentially due to the additional CH$_2$ spacer group available on **B** which adds extra flexibility to the molecule and enhances the adsorption. The computed structure and energetics indicate that absorption of the species **B** is thermodynamically favoured over **A**, in agreement with the experimental findings.[16]

The computed spin density plots for the NitR-**A**-SCH$_3$ and ^{3}NitR-**A**-S• are shown in Fig. 1 and the spin densities of the selected atoms are collected in Table 2. The spin densities of ^{3}NitR-**A**-S• are extensively delocalised on the surface gold atoms. The unadsorbed ^{3}NitR-**A**-S˙ species has the spin densities
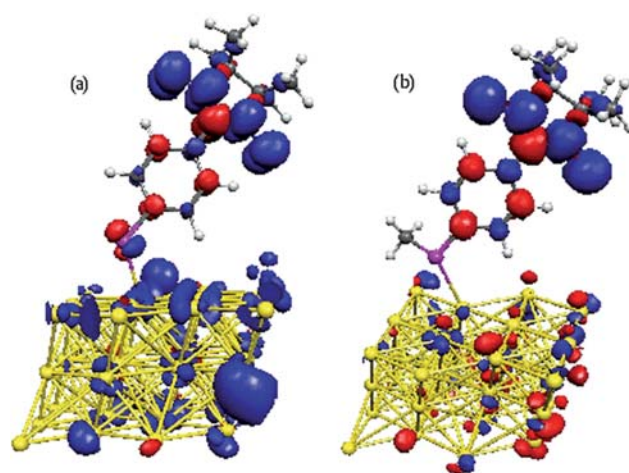

Fig. 1 The PDFT–TPSS computed spin density plots of (a) ^{3}NitR-**A**-S• and (b) ^{2}NitR-**A**-SCH$_3$. The blue colour represents positive spin density while the red represent negative spin densities.

of 0.761 on the sulfur atom and 0.260 and 0.270 on the two nitrogen atoms and 0.350 and 0.370 on the two oxygen atoms. The spin density on the NitR centre is extensively delocalised to both the N–O units with a significant negative spin density (−0.180) on the spacer carbon atom. This is the typical spin distribution observed in the NitR radicals.[19] The spin density on the sulfur atom dramatically diminishes on adsorption just to 0.223. On the other hand the spin densities on the NitR moiety are only slightly perturbed with 0.234 and 0.249 on the nitrogen atoms and 0.345 and 0.249 on the oxygen atoms. The difference in the spin densities between the two N–O groups is due to the small difference in N–O bond lengths (1.28 vs. 1.29 Å) arising due to the tilting of the molecule towards the Au(111) surface (see Fig. 1). The N–O group closer to the surface has shorter N–O bond length and larger spin densities. The decrease of the spin density on the sulfur atom reveals an extensive delocalisation of the spin densities to the Au(111) as it is apparent from Fig. 1. The gold atom with the shortest Au–S contact has in fact negative spin density (−0.011, see Table 2) indicating a predominant spin polarisation mechanism for the spin distribution to the Au(111).

Table 1 DFT computed energetic and structural information for the NitR-**A**-SCH$_3$ and NitR-**B**-SCH$_3$ species on Au(111). D is for S–Au(111) distance; Au–S is for the S distances from the closest Au atoms; and ζ is for the supplementary angle of C–S–Au(111) angle

Species	Position	D/Å	Au–S/Å	$\zeta/°$	ΔE^f/kcal mol^{-1}
^{2}Au$_{36}$-Nit-**A**-SCH$_3$	Quasi-atop	2.71	2.80	129.1	5.3
^{1}Au$_{36}$-Nit-**A**-S•	Quasi-atop	2.37	2.49	134.4	−17.0
^{3}Au$_{36}$-Nit-**A**-S•		2.37	2.49	133.9	−16.3
^{2}Au$_{36}$-Nit-**B**-SCH$_3$	Atop	2.31	2.31	105.0	−4.1
^{1}Au$_{36}$-Nit-**B**-S•	fcc-bridge	2.20	2.56; 2.76	132.3	−22.6
^{3}Au$_{36}$-Nit-**B**-S•	fcc-bridge	2.24	2.59; 2.80	131.0	−21.1
^{3}Au$_{36}$-Au$_{ad}$-Nit-**A**-SCH$_3$ (fcc)	Atop	2.45	2.45	113.2	−21.4
^{3}Au$_{36}$-Au$_{ad}$-Nit-**A**-S$^-$	Atop	2.37	2.37	112.8	−27.6
^{2}Au$_{36}$-Au$_{ad}$-Nit-**A**-S•	Atop	2.35	2.35	112.0	−41.1
^{4}Au$_{36}$-Au$_{ad}$-Nit-**A**-S•	Atop	2.35	2.35	112.5	−41.6
^{5}Au$_{54}$-(Au$_{ad}$-Nit-**B**-S CH$_3$)$_2$	Atop	2.54	2.54	110.4	−6.8
	Atop	2.52	2.52	108.5	
^{3}Au$_{54}$-(Au$_{ad}$-Nit-**B**-S•)$_2$	Atop	2.36	2.36	110.9	−34.2
	Atop	2.34	2.34	109.4	
^{2}Au$_{54}$-Nit-**B**-S•–Au$_{ad}$-Nit-**B**-S•	Atop–atop	2.73, 2.71	2.37, 2.55; 2.36, 2.61	113.7, 103.4	−37.7

Table 2 The PDFT (TPSS) computed Mulliken spin densities of selected atoms in NitR-A-SCH₃ and NitR-**B**-SCH₃ species. For the radical species the values given in the parenthesis is for the singlet state

Species (atom)	Au₃₆-NitR-A-SCH₃	Au₃₆^{3,1}-NitR-A-S•	Au₃₆-NitR-B-SCH₃	Au₃₆^{3,1}-NitR-B-S•	Au₃₇-NitR-A-SCH₃^a	Au₃₇^{4,2}-NitR-A-S•	Au₃₇-NitR-A-S⁻
S	0.014	0.223(−0.066)	−0.037	0.294(0.072)	0.004	0.196(−0.018)	−0.018
N1	0.252	0.234(0.205)	0.253	0.242(−0.244)	0.258	0.248(0.219)	0.259
N2	0.250	0.249(0.229)	0.238	0.221(−0.224)	0.250	0.245(0.184)	0.237
O1	0.329	0.345(0.310)	0.345	0.320(−0.325)	0.333	0.335(0.231)	0.346
O2	0.316	0.293(0.247)	0.322	0.298(−0.300)	0.333	0.319(0.274)	0.301
C1	−0.148	−0.147(−0.122)	−0.161	−0.155(0.158)	−0.156	−0.148(−0.110)	−0.129
C2	−0.016	−0.015(−0.012)	−0.015	−0.014(0.014)	−0.016	−0.015(−0.014)	−0.016
C3	0.013	−0.016(−0.015)	−0.012	−0.011(0.010)	−0.016	−0.015(−0.012)	−0.016
Au_near	−0.003	−0.011, 0.044	−0.013, −0.020	−0.066, −0.060	—	—	—
Au_ad	—	(−0.023, −0.062)	—	(−0.12, 0.014)	0.025	0.040(−0.017)	0.009

^a The spin density belongs to the low energy fcc structure.

The other longer Au–S contacts on the first layers have all positive spin density in the range of 0.07 to 0.004. The bond lengths given in parenthesis are for the triplet state of the corresponding species. For the undissociated species, the spin density on the sulfur is very small as one could expect while on the N–O's of the NitR group is relatively larger (see Table 2) than that of the radical species, revealing a less extent of delocalisation. The spin densities on the species **B** resemble the ones computed for **A** with the additional CH₂ group on the **A** having a spin density of ∼0.01 in the dissociated as well as the undissociated species.

Reconstructed surface

In order to gain understanding on the surface reconstruction energetics for the NitR species, calculations have been performed for NitR-**B**-SCH₃ with 1 : 1 Au_ad/NitR-**B**-SCH₃ models. As with simple thiols, the presence of Au_ad substantially lowers the formation energies with the NitR-**B**-SCH₃ species having the formation energies of −21.4 kcal mol⁻¹ with the Au_ad on the fcc site and −14.8 kcal mol⁻¹ with the Au_ad placed on the hcp site. The adsorption of dissociated species is much more favourable with the heterolytically cleaved ³NitR-**B**-S⁻ species having the formation energy of −27.6 kcal mol⁻¹.

The homolytic cleavage leads to two different spin states, since the Au_ad also possesses an unpaired spin and the NitR-**B**-S• possesses two unpaired electrons: an all spin-up state leads to a quartet (⁴Au_ad-NitR-**B**-S•) while alternating spin down leads to a doublet (²Au_ad-NitR-**B**-S•) state. The formation energies are found to be −41.1 and −41.7 kcal mol⁻¹ for the doublet and quartet states respectively, the quartet being the ground state. Selected structural parameters are given in Table 1. The Au_ad–S bond distances in the undissociated species are 2.44 and 2.49 Å for the fcc and hcp site, respectively, while the NitR-**B**-S⁻ has 2.36 Å and the NitR-**B**-S• species have 2.348 and 2.349 Å for the quartet and doublet, respectively. This indicates that the formation energies are related to the strength of the Au_ad–S bond with the following pattern ³Au_ad-NitR-**B**-SCH₃ < ³Au_ad-NitR-**B**-S⁻ < ²Au_ad-NitR-**B**-S• <⁴Au_ad-NitR-**B**-S•. The computed spin densities (Table 2) here reveal similar pattern to that of the unreconstructed surface. Due to short and strong Au_ad–S bond, the spin density on the sulfur head diminished compared to that of the unreconstructed surface (0.223 vs. 0.196).

SAM structures

In order to shed some lights on the geometry of the SAM arrangements on the Au(111) surface, we focused our attention on newly collected STM images of Nit-**B**-S-CH₃ species (see ESI†, Fig. 2a and b), which is supposed to give the most ordered and stable experimental SAM.[16]

Considering the results obtained for simple thiols[21] and NitRs, we chose to concentrate our attention only on the reconstructed Au(111) surface. Fig. 2c gives basically the following information: (1) the Nit-**B**-S• is attached orthogonally with respect to the Au(111) surface and (2) a hexagonal-like lattice is present (see Fig. 2b). Considering the sampling of the distances of lengths A, B, and C reported in Fig. 2a as limits for the symmetry and the dimension of the possible cell to be used in the calculations we

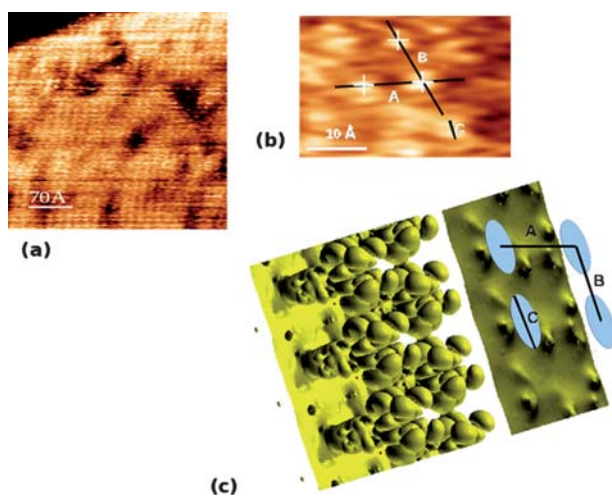**Fig. 2** (a) Experimental STM image (see ESI†). (b) Zoomed experimental STM image. A and B are the intermolecular distances between the spots. C is the measure of the wideness of the spots. $A = 9.6(10)$ Å; $B = 8.1(10)$ Å; and $C = 3.3–5.4$ Å. (c) Calculated STM images for the 1 : 1 Au_{ad}/thiol ratio model of NitR-**B**-S˙ species. $A = 8.95$ Å, $B = 8.66$ Å, and $C = 4.70$ Å.
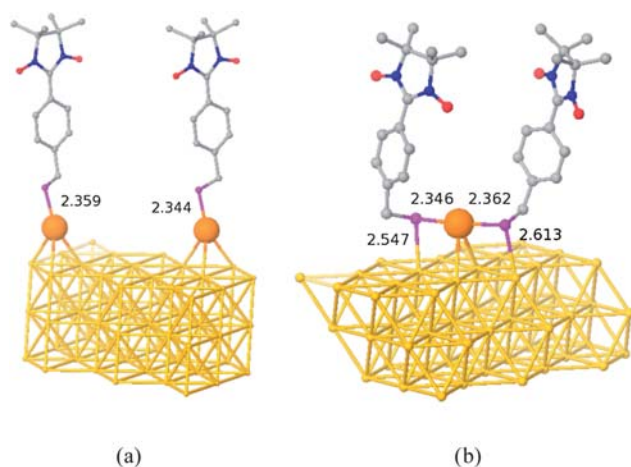

Fig. 3 The DFT computed structures for Au_{56} (a) and Au_{90} model (b) of the NitR-B species.

converged onto the two cells reported in Fig. 3: the 1 : 1 (a) and 1 : 2 (b) Au_{ad}/thiol model cells, respectively. In both cases, the calculations have been performed on the high spin state. For the 1 : 1 model the formation energy is -34.2 kcal mol^{-1}. The Au_{ad} occupies a hcp site and the ^{3}NitR-**B**-S• species adopt a *quasi*-atop configuration with the Au–S bond length of 2.35 Å. Likewise in the simple thiol radical species, the ^{3}NitR-**B**-S• has short (slightly longer: ~0.05 Å) and strong Au–S bond leading to very exothermic formation energies. The 1 : 2 model yields the formation energy of -37.7 kcal mol^{-1} for the ^{3}NitR-**B**-S• species having the NitR groups in the *cis* configuration. The structures resemble those of the simple thiols[19,41,42] with the *quasi*-atop configuration respect to the gold atoms on the Au(111) surface (in this case a hexagonal Au_{90} cell has to be used to reproduce the hexagonal lattice of adatoms). The surface structure of 1 : 1 and 1 : 2 Au_{ad}/thiol models is shown in Fig. 4. Since the structural
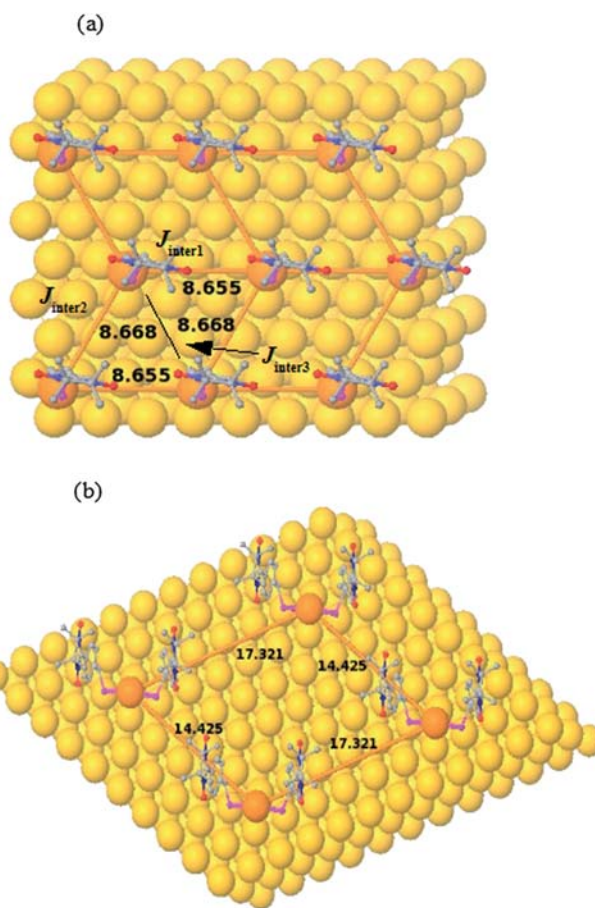

Fig. 4 A larger cell structure revealing the intermolecular distance in the (a) 1 : 1 (3 × 3) and (b) 1 : 2 Au_{ad}/thiol ratio models (6 × 4).

data given by the experimental STM image (see Fig. 2b) seem to be consistent with the 1 : 1 Au_{ad}/thiol model, we calculated STM images considering states between 0.2 eV and the Fermi energy. The bias employed here is in good agreement with the bias employed in the experimental STM measurement (see ESI†). The computed STM image for this structure reveals a regular pattern as observed in the experiment and suggests that spots can be originated by the NitRs N–O group electron densities. This is not surprising given the fact that the unpaired electron of the NitR resides in the partly occupied bands across the Fermi energy. Additionally, from the experimental STM images of NitR-**B** species, we have computed the radius of the oval shaped spots in the range of ~4.5 Å that agrees with the O···O distance between the two nitronyl NO groups (distance A in Fig. 2b) of the computed structures (averaged 4.7 Å). Additionally there are two intermolecular distances, one corresponding to the distance between the spot centers of NitR group facing each other (distance B in Fig. 2b) and another corresponding to NitR group lying adjacent to each other: 8.93 Å (computed) *vs.* 9.6(10) Å (experimental) and 8.61 Å (computed) *vs.* 8.1(10) Å (experimental). The agreement is evident.

Magnetic properties of SAM structure

Although the magnetic properties of the isolated NitR are well understood,[35] the magnetic properties of these species on the

Au(111) are still elusive. Experimentally EPR spectroscopy has been employed to probe its magnetic properties. However, the extremely small quantity of sample in the SAM (often close to the sensitivity limit of the EPR) makes the interpretation of the spectra a challenging task. For species **A**, clean EPR spectra were recorded[16] which indicate that the radical centres are intact. The sample prepared by drop casting and successive evaporation of the solvents gives different EPR spectra where the hyperfine structure of nitrogens is lost indicating a strong intermolecular interaction. Further the SAMs prepared from a disulfur NitR-**A**-S-S-**A**-NitR precursor result in the adsorption of NitR-**A**-S• species and an anisotropic *g* was found indicating a vertical adsorption on the surface.[17] Some DFT calculations have been reported for this structure to compute the intramolecular magnetic exchange interaction on a very simple gold layer model, and these calculations also indicate a very strong ferromagnetic exchange between the two radical centres.[38,39] The structure employed for the calculation of exchange interaction is, however, unrealistic.

From our calculations on different model structures, it is clear that there is residual spin density on the sulfur atom, especially for the dissociated radical species. The spin density on the sulfur atom, however, diminishes upon adsorption and the spin density is thus largely delocalised on the Au(111). This is true more for the reconstructed than for the unreconstructed surfaces. An extensive delocalisation of the spin density on the gold surface is present even at large intermolecular distances. Therefore, the NitRs are expected to be coupled through magnetic exchange interactions.

The magnetic exchange interaction is very sensitive to the exchange-correlation functional, and in several instances we have demonstrated that in general hybrid functionals such as B3LYP[32] provide good estimates of the *J* values. Therefore, here we perform calculations using B3LYP functional on the TPSS computed geometries with Jaguar suite of programmes and our calculations are limited to species **B** (^{1,3}NitR-**B**-S•).

Our initial focus is to calculate the intramolecular exchange interaction (J_{intra}) between the NitR moiety and the sulfur radicals in NitR-**B**-S• species. Therefore, we have chosen two possible C_{ar}–C_{ar}–C_{al}–S (C_{ar}=$C_{aromatic}$ and C_{al}=$C_{aliphatic}$) dihedral angles, NitR-**B1**-S• and NitR-**B2**-S• (see Fig. 5). Therefore, we have computed the J_{intra} for both the species. The exact tech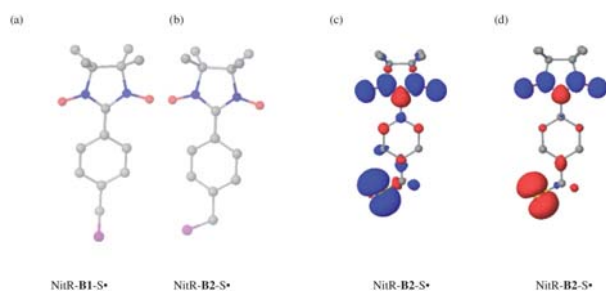nical details of the calculation of the magnetic exchange are described elsewhere[35] with some details relevant to the present systems provided in the ESI†.

The calculations on **B1** and **B2** without any gold atoms give a ferromagnetic J_{intra} with -246.6 cm^{-1} for **B1** and -69.0 cm^{-1} for **B2** (using $H = J\mathbf{S_1}\bullet\mathbf{S_2}$ formalism). A large J_{intra} observed is due to the presence of unpaired electrons on the orthogonal π-type orbitals in both centres (see Fig. 5). The large difference in the strength of the magnetic exchange between **B1** and **B2** arises essentially due to the dihedral angle as revealed by the plot of J_{intra} *vs.* the dihedral angle for **B2** species. This plot gives a sin^2 shaped curve with J_{intra} increases with increasing the dihedral angle and reaches a maximum at 90° with the J_{intra} of -348.9 cm^{-1}. The spin density plots of single and triplet state shown in Fig. 5 reveal that the predominant mechanism of spin distribution is spin polarisation as the spacer atoms have alternating signs. To understand the effect of gold layer on the J_{intra}, calculations have been performed on both **B1** and **B2** with single gold layer having 20 gold atoms with no adatoms. This yields the magnetic exchange of -311.3 cm^{-1} and -32.8 cm^{-1} for **B1** and **B2**, respectively. These numbers are different from those of the free fragments and the difference is due to the delocalisation of the spin density of sulfur atoms to the gold layer. The decrease in the magnitude of spin density on the sulfur atom (0.548 *vs.* 0.966 for adsorbed and unadsorbed sulfur atom) upon adsorption raises the ferromagnetic J_{intra} only for **B1**, yet the trend of larger J_{intra} for large dihedral remains. The large J_{intra} observed in the gas phase is maintained even after NitR is adsorbed on the gold surface This has also been previously reported for the radical species type **A** (NitR-**A**-S•) but on unrealistic models containing only a few gold atoms.[39,40]

In the next step we have computed the intermolecular exchange interaction between the NitR-**B**-S• units in the gold lattice. The chosen molecular arrangement was one of the 1 : 1 Au$_{ad}$/NitR-**B**-S• ratio model. Due to the large size of the molecule and possible SCF convergence problems due to the extensive delocalisation of unpaired electrons to the gold atoms, calculations have been performed within the dimer approximation[33] to compute the exchange interactions reported in Fig. 4a in addition to the J_{intra}. The calculations performed on a dimer model on 1 : 1 Au$_{ad}$/NitR-**B**-S• ratio model reveal a ferromagnetic J_{intra} = -108.7 cm^{-1} in line with what found with the clean surface. Regarding the J_{inter}, three possible different short magnetic exchange interactions depending on the orientation and Au$_{ad}$–Au$_{ad}$ distance are possible (see Fig. 4a). The calculation yields J_{inter1} = -16.7 cm^{-1}, J_{inter2} = 5.7 cm^{-1}, and J_{inter3} = 23.0 cm^{-1}. Only the J_{inter1} is ferromagnetic while the other two are antiferromagnetic. J_{inter1} which is the exchange between the two NitR next to each other with a short O···O (matching oxygens of the two distinct NitRs) distance is ferromagnetic while other two interactions with relatively longer O···O distance are antiferromagnetic. The large computed exchange interactions indicate that the gold layer in fact acts as a super-exchange medium. Efficient spin delocalisation on the gold layer can, therefore, be the reason of a stronger intermolecular coupling. The strength and the nature of this three intermolecular interactions essentially lead to a ferromagnetic coupling between the very first-neighbors *versus* an antiferromagnetic coupling between next nearest-neighbors NitRs (see Fig. 4a) with an $S = 0$ as the spin ground state for this tetramer. The sensitivity of the magnetic

Fig. 5 The structure of (a) NitR-**B1**-S• and (b) NitR-**B2**-S• species with different C_{ar}–C_{ar}–C_{al}–S dihedral angle together with the (c) triplet and (d) singlet spin density plots of NitR-**B2**-S• species.

properties of the organic moieties to spin delocalization in the metal is extremely exciting for molecular spintronics developments. Experimental checks are needed.

For 1 : 2 Au_{ad}/NitR-**B**-S• ratio model we have computed only the J_{inter} molecular exchange within the dimeric unit which resulted to be antiferromagnetic with $J_{inter} = 2.4$ cm^{-1}. This interaction is weaker compared to the J_{inter1} computed for the 1 : 1 Au_{ad}/NitR-**B**-S• ratio model.

4. Conclusions

The design and realization of ordered systems of magnetic molecules are one of the challenges of molecular nano-magnetism. The self-assembled monolayers offer many opportunities to organize different types of magnetic molecules on different substrates.

Likewise in the alkylthiols, the NitR radical species are found to be energetically favourable. The formation of radical centre here presents an unexpected twist as the two radical centres, NitR and S• could be coupled leading to different spin states. The computed spin densities on this species reveal an extensive delocalisation of electrons to the Au(111) much larger in magnitude than that of the alkylthiols for apparent reasons. This spin distribution can be addressed for the strong intermolecular coupling. The reconstructed surface with Au_{ad} leads to additional spin states and ^{3}NitR-**B**-S•-Au-^{3}NitR-**B**-S• type species is found to be energetically favourable. The magnetic exchange interactions present in the SAMs were evaluated for intra- and inter-molecular couplings. Such magnetic characterization we presented in the paper does not have any precedent at this level of approximations for SAM of NitR's to our knowledge.

The next step on the use of NitR as models of the behaviour of organized magnetic molecules will be addressed to the structural and magnetic dynamics with experiments with pulsed EPR to monitor the spin dynamics and DFT calculations investigating the restricted molecular motion responsible of the observed behaviour.

Acknowledgements

References

1 A. Ulman, *Chem. Rev.*, 1996, **96**, 1533; A. Ulman, *Acc. Chem. Res.*, 2001, **34**, 855.

2 G. E. Poirier, *Chem. Rev.*, 1997, **97**, 1117.

3 J. C. Love, L. A. Estroff, J. K. Kriebel, R. G. Nuzzo and G. M. Whitesides, *Chem. Rev.*, 2005, **105**, 1103; A. Kumar, N. L. Abbott, H. A. Biebuyck, K. Enoc and G. M. Whitesides, *Acc. Chem. Res.*, 1995, **28**, 219.

4 G. Heimel, L. Romaner, E. Zojer and J.-L. Bredas, *Acc. Chem. Res.*, 2008, **41**, 721.

5 J. E. Houston and I. H. Kim, *Acc. Chem. Res.*, 2002, **35**, 547.

6 D. P. Woodruff, *Phys. Chem. Chem. Phys.*, 2006, **10**, 7211.

7 C. Vericat, M. E. Vela, G. A. Benitez, J. A. M. Gago, X. Torrelles and R. C. Salvarezza, *J. Phys.: Condens. Matter*, 2006, **18**, 867.

8 A. Cornia, A. Fabretti, M. Pacchioni, L. Zobbi, D. Bonacchi, A. Caneschi, D. Gatteschi, R. Biagi, U. Del Pennino, V. De Renzi,

L. Gurevich and H. S. J. Van der Zant, *Angew. Chem., Int. Ed.*, 2003, **42**, 1645.

9 M. Mannini, F. Pineider, P. Sainctavit, L. Joly, A. Fraile-Rodriguez, M.-A. Arrio, C. Moulin, C. Dit, W. Wernsdorfer, A. Cornia, D. Gatteschi and R. Sessoli, *Adv. Mater.*, 2009, **21**, 167.

10 M. Mannini, P. Sainctavit, R. Sessoli, D. M. Cartier, F. Pineider, M.-A. Arrio, A. Cornia and D. Gatteschi, *Chem.–Eur. J.*, 2008, **14**, 7530.

11 M. Fonin, S. Voss, M. Burgert, Y. S. Dedkov, U. Groth and U. Ruediger, *J. Phys.: Conf. Ser.*, 2008, **100**, 52070.

12 S. Voss, M. Burgert, M. Fonin, U. Groth and U. Ruediger, *Dalton Trans.*, 2008, 499.

13 S. Barraza-Lopez, M. C. Avery and K. Park, *Phys. Rev. B: Condens. Matter Mater. Phys.*, 2007, **76**, 224413.

14 E. Coronado, A. Forment-Aliaga, F. M. Romero, V. Corradini, R. Biagi, V. De Renzi, A. Gambardella and U. Del Pennino, *Inorg. Chem.*, 2005, **44**, 7693.

15 M. Mannini, F. Pineider, P. Sainctavit, C. Danieli, E. Otero, C. Sciancalepore, A. M. Talarico, M.-A. Arrio, A. Cornia, D. Gatteschi and R. Sessoli, *Nat. Mater.*, 2009, **8**, 194; M. Mannini, F. Pineider, C. Danieli, F. Totti, L. Sorace, Ph. Sainctavit, M.-A. Arrio, E. Otero, L. Joly, J. Criginski Cezar, A. Corina and R. Sessoli, *Nature*, DOI: 10.1038/nature09478.

16 M. Mannini, L. Sorace, L. Gorini, F. M. Piras, A. Caneschi, A. Magnani, S. Menichetti and D. Gatteschi, *Langmuir*, 2007, **23**, 2389.

17 M. Matsushita, N. Ozaki, T. Sugawara, F. Nakamura and M. Hara, *Chem. Lett.*, 2002, 596.

18 G. Harada, H. Sakurai, M. Matsushita, A. Izuoka and T. Sugawara, *Chem. Lett.*, 2002, 1030.

19 K. Bernot, J. Luzon, L. Bogani, M. Etienne, C. Sangregorio, M. Shanmugam, A. Caneschi, R. Sessoli and D. Gatteschi, *J. Am. Chem. Soc.*, 2009, **131**, 5573, and references therein; J. H. Osiecki and E. F. Ullman, *J. Am. Chem. Soc.*, 1968, **90**, 1078; M. Tamura, Y. Nakazawa, D. Shiomi, Y. Nozawa, M. Hosokoshi, M. Ishikawa and M. Kinoshita, *Chem. Phys. Lett.*, 1991, **186**, 401; R. Chiarelli, M. A. Novak, A. Rassat and J. L. Tholence, *Nature*, 1993, **363**, 147.

20 M. Mannini, D. Rovai, L. Sorace, A. Perl, B. J. Ravoo, D. N. Reinhoudt and A. Caneschi, *Inorg. Chim. Acta*, 2008, **361**, 3525.

21 A. Bencini, G. Rajaraman, F. Totti and M. Tusa, *Superlattices Microstruct.*, 2009, **46**, 4; G. Rajaraman, A. Caneschi, D. Gatteschi and F. Totti, *J. Phys. Chem.*, 2010, submitted.

22 J. VandeVondele, M. Krack, F. Mohamed, M. Parrinello, T. Chassaing and J. Hutter, *Comput. Phys. Commun.*, 2005, **167**, 103.

23 G. Lippert, J. Hutter and M. Parrinello, *Mol. Phys.*, 1997, **92**, 477.

24 G. Lippert, J. Hutter and M. Parrinello, *Theor. Chem. Acc.*, 1999, **103**, 124.

25 R. C. Hoft, M. J. Ford, A. M. McDonagh and M. B. Cortie, *J. Phys. Chem. C*, 2007, **111**, 13886.

26 J. Tao, J. P. Perdew, V. N. Staroverov and G. E. Scuseria, *Phys. Rev. Lett.*, 2003, **91**, 146401; A. Ruzsinszky, J. P. Perdew and G. I. Csonka, *J. Phys. Chem. A*, 2005, **109**, 11015.

27 A. Vargas, G. Santarossa, M. Lannuzzi and A. Baiker, *J. Phys. Chem. C*, 2008, **112**, 10200.

28 G. Santarossa, A. Vargas, M. Iannuzzi, C. A. Pignedoli, D. Passerone and A. Baiker, *J. Chem. Phys.*, 2008, **129**, 234703.

29 A. Ferral, E. M. Patrito and P. Paredes-Olivera, *J. Phys. Chem. B*, 2006, **110**, 17050; Y. Yourdshahyan, H. K. Zhang and A. M. Rappe, *Phys. Rev. B: Condens. Matter Mater. Phys.*, 2001, **63**, 81405.

30 A. Nogoya and Y. Morikawa, *J. Chem. Phys.*, 2007, **19**, 365245.

31 *Jaguar 7.0*, Schrödinger, Portland, OR 97204.

32 A. D. Becke, *J. Chem. Phys.*, 1993, **98**, 5648; P. J. Stephens, F. J. Devlin, C. F. Chabalowski and M. J. Frisch, *J. Phys. Chem.*, 1994, **98**, 11623.

33 P. J. Hay and W. R. Wadt, *J. Chem. Phys.*, 1985, **82**, 270; P. J. Hay and W. R. Wadt, *J. Chem. Phys.*, 1985, **82**, 284; P. J. Hay and W. R. Wadt, *J. Chem. Phys.*, 1985, **82**, 299.

34 P. C. Hariharan and J. A. Pople, *Theor. Chim. Acta*, 1973, **28**, 213; M. M. Francl, W. J. Petro, W. J. Hehre, J. S. Binkley, M. S. Gordon, D. J. DeFrees and J. A. Pople, *J. Chem. Phys.*,

1982, **77**, 3654; V. Rassolov, J. A. Pople, M. Ratner and T. L. Windus, *J. Chem. Phys.*, 1998, **109**, 1223.

35 A. Bencini and F. Totti, *Int. J. Quantum Chem.*, 2005, **101**, 819; A. Bencini and F. Totti, *J. Chem. Theory Comput.*, 2009, **5**, 144.

36 L. Kankate, A. Turchanin and A. Goelzhauser, *Langmuir*, 2009, **25**, 10435.

37 G. Rajaraman, F. Totti, A. Caneschi and D. Gatteschi, in preparation.

38 Y. Hyeon, Y. Kwan and K. Kim, *J. Phys. Chem.*, 1990, **94**, 2552; C. J. Sandroff and D. R. Herschbach, *J. Phys. Chem.*, 1982, **86**, 3277; K. L. Kim, S. J. Lee and K. Kim, *J. Phys. Chem. B*, 2004, **108**, 9216.

39 M. Okumura, Y. Kitagawa, T. Kawakami, T. Taniguchi and K. Yamaguchi, *Synth. Met.*, 2005, **154**, 313; M. Okumura, Y. Kitagawa, T. Takeshi and K. Yamaguchi, *Polyhedron*, 2005, **24**, 2330.

40 M. Okumura, Y. Kitagawa, T. Kawakami and K. Yamaguchi, *Polyhedron*, 2007, **26**, 2179.

41 H. Grönbeck and H. Häkkinen, *J. Phys. Chem. B*, 2007, **111**, 3325.

42 A. Chaudhuri, T. J. Lerotholi, D. C. Jackson, D. P. Woodruff and R. G. Jones, *Phys. Rev. B: Condens. Matter Mater. Phys.*, 2009, **79**, 195439; A. Chaudhuri, T. J. Lerotholi, D. C. Jackson, D. P. Woodruff and V. Dhanak, *Phys. Rev. Lett.*, 2009, **102**, 126101.